Journal Name

ARTICLE

Systematic Investigation of Self-Organization Behavior in Supramolecular π-Conjugated Polymer for Multi-color Electroluminescence

Received 00th January 20xx,
Accepted 00th January 20xx

DOI: 10.1039/x0xx00000x

www.rsc.org/

Jin-Yi Lin,[a,c,f†] Bin Liu,[b†] Meng-Na Yu,[b] Xu-Hua Wang,[c] Lu-Bing Bai,[a] Ya-Min Han,[a] Chang-Jin Ou,[a] Ling-Hai Xie,*[b] Feng Liu,[a] Wen-Sai Zhu,[a] Xin-Wen Zhang,*[b] Hai-Feng Ling,[b] Paul N. Stavrinou,[d] Jian-Pu Wang,[a] Donal D. C. Bradley*[e] and Wei Huang*[a,b,f]

The nature of the chain aggregation in solution always results into variable spin-coated film mesoscale morphology and uncontrollable device performance. The abundant variety and increasing chemical complexity of conjugated polymers induced additional diverse electrostatic and dispersion interactions (non-covalent interaction), although it is not fully understood how the interplay of these forces results in observed conformational order, chain aggregates and film morphologies. Herein, we present a precise study on the role of non-covalent interaction in self-organization behavior, conformational order and optoelectrical property of polyfluorene (PPFOH) toward tuning their electroluminescence (EL). Supramolecular PPFOH system consisted of a intrinsically doped hydrogen-bond-assisted microstructures as a "guest" and blue light-emitting backbone chain as a "host", which show a special binary emissive property of solution-induced self-dopant formation in the amorphous films. As a result of a strong non-covalent interaction between polymer chains and solvent molecules (type II solvent), likely distorted or fold chain in rod-coil or branch cluster show a narrow and strong aggregation emission at 525~540 nm. And low-polar solvents (called type I) can also induce a shoulder low-energy emission at 550~580 nm in the films, attributed to the extended and stretched chain complex for the tendency of interchain hydrogen-bonding interaction. Further evidences from nanoscale infrared (AFM-IR) analysis confirmed the stronger hydrogen-bonding interaction in the type II films than those in type I films. Finally, supramolecular PPFOH electroluminescence colours can tune from blue, sky blue, green, white, yellow to orange.

Introduction

Conjugated polymers (CPs), as one important class of semiconductor materials, have a series of unique advantages compared to inorganic semiconductors such as easily tailored mechanical, electrical and optical properties and soluble in common solvents for large area processing, thereby enabling the fabrications of flexible devices such as polymer light emitting diodes (PLEDs), organic solar cells (OSC) and organic transistors.[1] Device performance is strongly affected by the film morphology that governs the exciton and charge carrier properties in the solid states.[2] In general, the microstructures of solution-processed CPs films can be varied from semi-crystalline structures, ordered aggregates to amorphous states since CPs are weakly bonded macromolecules with numerous degrees of conformational freedom.[3] Actually, film morphology are influenced by not only solution-processing technology or solution formulations[4] but also film post-processing such as thermal or solvent treatments.[5] Precursory aggregate in the solution dominates the chain rearrangement in the film-casting process and film morphology, which further influenced on excimer/exciplex formation, Förster energy transfer and exciton diffusion.[2a, 3c, 6] In this regard, CPs films with aggregation structures are associated with the chain conformation and diversity, complex electrostatic and dispersion interactions in the solution.[3c, 7] In this work, we focus on the study of CPs self-organization behavior in solutions to explore their effect on spun film morphology and devices performance toward precisely tuning electroluminescence (EL) property.

[a.] Key Laboratory of Flexible Electronics (KLOFE) & Institute of Advanced Materials (IAM), Jiangsu National Synergetic Innovation Center for Advanced Materials (SICAM), Nanjing Tech University (NanjingTech), 30 South Puzhu Road, Nanjing, China. E-mail: wei-huang@njtech.edu.cn
[b.] Key Laboratory for Organic Electronics and Information Displays & Institute of Advanced Materials (IAM), Jiangsu National Synergetic Innovation Center for Advanced Materials (SICAM), Nanjing University of Posts & Telecommunications, 9 Wenyuan Road, Nanjing, China. E-mail: iamlhxie@njupt.edu.cn, iamxwzhang@njupt.edu.cn
[c.] Department of Physics and Centre for Plastic Electronics, The Blackett Laboratory, Imperial College London, Prince Consort Road, London SW7 2AZ, UK
[d.] Department of Engineering Science, University of Oxford, Parks Road, Oxford OX1 3PJ, UK
[e.] Departments of Engineering Science and Physics and Mathematical, Physical and Life Sciences Division, University of Oxford, 9 Parks Road, Oxford OX1 3PD, UK. E-mail: donal.bradley@mpls.ox.ac.uk
[f.] Shaanxi Institute of Flexible Electronics (SIFE), Northwestern Polytechnical University (NPU), 127 West Youyi Road, Xi'an, Shaanxi710072, China.
† Jin-Yi Lin, Bin Liu contributed equally to this work.

Electronic Supplementary Information (ESI) available: [details of any supplementary information available should be included here]. See DOI: 10.1039/x0xx00000x

In general, CPs are organic macromolecules featured by a backbone chain with a system of delocalized π-electrons that can lead to diverse electrostatic and secondary interactions such as aromatic π-π, hydrogen bonding and chalcogen-chalcogen interaction.[3b, 6e, 8] These secondary interactions are widely exist in solution and film states, which further determine chain conformational order and film morphology.[6e, 7a, 9] Even a weak interaction between chain to chain such as Van der Waals' force is enough to form a large scale of regular aggregates, thus the close-packing of the chromophores can significantly influence the molecular geometry, altering mobility, color and emission efficiency.[10] These synergistic effects of interchain and chain-solvent interaction or solvation primarily determined the chain aggregation behavior to allow for self-assembling into varied mesoscale conformational types, such as globule, stacked rod or toroid.[3c, 6b, 11] Therefore, an effective strategy to improve and tune the optoelectrical property of CPs is to precisely tune the aggregation behavior via controlling non-covalent interactions in a solution and further optimize their film morphology.

As one of the most studied light-emitting CPs (LCPs), polyfluorene is widely investigated in the PLEDs and organic lasers due to their relatively easy to modify the chemical structure, deep-blue emission and high photoluminance quantum yield (PLQY).[1d, 3c, 12] In the previous works, we observed that fluorine-based materials with a supramolecular hydrogen-bonding interaction show diverse molecular arrangement, conformational order and aggregation behavior in the solution, crystal and films.[6a, 6e, 6h] Herein, we systemically investigate a "programmable" aggregation behavior of supramolecular PPFOH (*Scheme 1*) in the precursor solutions toward controlling the film morphology to tune their EL property. Such supramolecular PPFOH system consisted of a intrinsically aggregate as a "guest" and blue light-emitting backbone chain of polyfluorenes as a "host", and exhibited a special dynamic "binary" emissive behavior. As the results of different conformational orders and aggregation structures, PPFOH has two types of chain complex in solution states: one is chain to chain interaction, and another is chain to solvent interaction, that leads to two type aggregation-induced emissions. Finally, EL colors from blue, white, green, yellow to orange was achieved via supramolecular approach.

Results and Discussion

Structural Characterization and Fundamental Property of PPFOH. PPFOH and poly(9-(octyloxy)-9-(4-(octyloxy)phenyl)-2,7-fluorene) (PPFO8) without the hydroxyl units were synthesized via Yamamoto polymerization. Gel permeation chromatography (GPC) shows that PPFOH and PPFO8 have a number-average molecular weight (M_n) and polydispersity index (PDI) of about 2.14 × 10^4 and 1.68, 6.92 × 10^4 and 1.62, respectively (Figure S1). It is deduced that the degree of polymerization (DP) for PPFOH and PPFO8 are estimated to be *c. a.* 55 and 139. Meanwhile, it was noticed that the featured peak of ketone at 1720 cm^{-1} is not appeared in the Fourier transform infrared (FTIR) spectroscopy of PPFOH powder (Figure S2).[13] The incorporation of hydroxyl group into the molecule design affords PPFOH to have an excellent solubility and amphiphilic property in tetrahydrofuran (THF), 1, 4-dioxane (DOX) and N,N-dimethyl formamide (DMF) (contained heteroatoms: O, with available alone pairs of electrons) for the formation of hydrogen bonds between polymer chain and solvents.[11b] PPFOH has relative poor solubility in organic low polar solvents such as chloroform ($CHCl_3$), toluene and 1,2-dichloroethane (DCE). The thermo gravimetric analyzer (TGA) and differential scanning calorimetry (DSC) curves of the PPFOH are shown in Figures S3 and S4. The 5% weight loss temperature (T_d) of the PPFOH is above 340 °C and the glass transition temperatures (T_g) is ~120 °C. No other phase transition can be found in the DSC curves. The cyclic voltammetry (CV) curve of PPFOH is shown in Figure S5. The onset oxidation potential (1.11 V) and the onset reduction potential (-2.23 V) are obtained directly from the curve, and then the highest occupied molecular orbital (HOMO) (5.91 eV) and lowest unoccupied molecular orbital (LUMO) (-2.57 eV) levels are calculated from the equations E_{HOMO} = -(E_{ox}-E_{FOC})-4.8 eV and E_{LUMO} =-(E_{red}-E_{FOC})-4.8 eV.

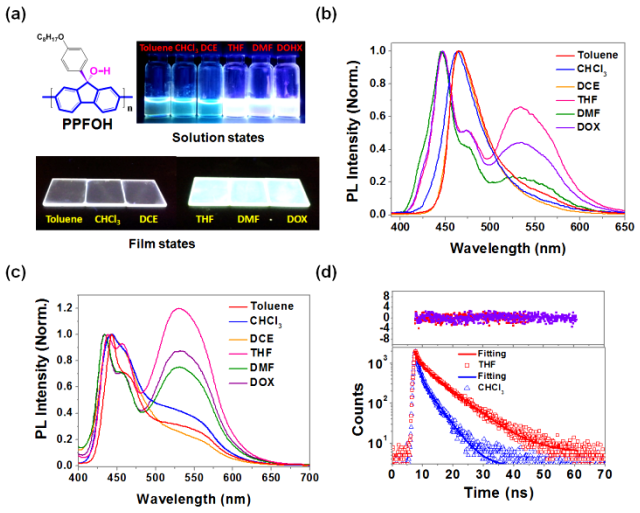

Figure 1. (a) Chemical structure of PPFOH and photographs of PPFOH in various precursor solutions (5 mg/ml) and films under UV light (365 nm). PL spectra of PPFOH with various solutions (b) and (c) spin-coated films. PL spectra of precursor solutions (5 mg/ml) are measured by using the front-face detection from a 1 mm cuvette to extremely minimize the effect of self-absorbance on PL spectra. (d) Transient decay spectra of PPFOH various films. Detected wavelengths are both at 555 nm.

Aggregation Behavior of PPFOH in Various Solutions and Films. In order to investigate the supramolecular aggregation behavior, photoluminescence (PL) spectra of PPFOH in six solvents with the same concentration of 5 mg/ml, and their corresponding spin-coated films are shown in **Figure 1**. We can observed that PPFOH in toluene, DCE and $CHCl_3$ solutions (Defined as a Type I solvent) showed sky blue emission. However, once PPFOH are dissolved in THF, DOX and DMF (Defined as Type II solvents), and emission colors were changed to yellow-green And the spin-coated films from two

Journal Name

ARTICLE

Table 1. Photophysical data of PPFOH in type I ($CHCl_3$) and type II (THF) solution, together with corresponding spin-coated films.

Polymer	Solvent	State	λ_{abs} (nm)	λ_{PL} (nm)	τ (ns)	ϕ_{PLQY} (%)[c]	Emitting colour
PPFOH	THF	Solution[a]	384	447, 473, 528	5.60	36	Nearly white
		Film[b]	390	438, 456, 533	6.86	18	Yellow-green
	$CHCl_3$	Solution[a]	390	465	0.54	28	Sky blue
		Film[b]	395	441, 560	2.97	13.3	Pink
PPFO8	$CHCl_3$/THF	Film	390	421, 446, 476	0.42	45/43	Deep-blue

[a]Concentration of 5 mg/ml. [b]Spin-coated films. [c]PFO amorphous film with Φ_{PLQY} of about 43% at the same conditions.

type solutions give pink (type I) and green-yellow (type II) color emissions, respectively (Figure 1a). Under the condition of a solution that minimize the self-absorbance, PL spectra of PPFOH in type I solutions have one only emission peak at 465 nm for a strong interchain hydrogen-bonding interaction in solution (Figure 1b).[6a] In contrast, PL spectra of PPFOH in type II solutions have three emission peaks at 447, 473 and 528 nm assigning to the 0-0, 0-1 intra-chain singlet transition and aggregation or excimer emission as results of PPFOH amphiphilic property.[14] Furthermore, the emission spectra of films spin-coating from both two type solutions, have a special dynamic "binary" emissive behavior, in which one is in the blue emission at 440~460 nm and the other is the green emission at 520~560 nm. There is a narrow and sharp emission at 525-530 nm for the PPFOH type II films. This long-wavelength emission is similar to the ones from amphiphilic oligofluorene or polyfluorene, also further confirmed the amphiphilic property of PPFOH in type II solution.[14] However, the PL spectra of PPFOH type I films have a shoulder peak at 550-560 nm, which has the same spectra from the cross-linked poly(9,9-dioctylfluorene) (PFO) gelation structure.[6f, 6h, 10c] Corresponding maximum absorption peaks are about 385 386 (DOX), 388 (DMF) and 390 (DCE), 392 ($CHCl_3$), 396 nm (Toluene) (Figure S6), suggested a longer effective conjugated length for the extended chain conformation formed in Type I films than those in type II films. However, the emission spectra of PPFO8 model polymer films spin-coated from toluene, $CHCl_3$ and THF solutions, consisted of similar three emission peaks at 421, 446 and 476 nm assigned to the 0-0, 0-1 and 0-2 intrachain singlet transitions due to the isotropic phase (Figure S7).[10c] Meanwhile, the lifetime decays for both two types of green emissions exhibit double-exponential, contributing to the singlet transitions of single-chain and molecular aggregation or excimer (Figure 1d). The life times of PPFOH type I films are calculated about 1.01 ns (24%) and 2.97 ns (76%) at 555 nm. However, the PPFOH type II films, show two life decay times of 0.95 ns (36%) and 6.86 ns (64%) at 555 nm. Therefore, it can be effective concluded that there are two different self-organization behaviors with two types of the low energy band emissions for the different non-covalent interactions in the solution and film states.

Static/Dynamic light scattering (SLS/DLS) were used to explore the differences and related inherent regularity in these two solutions at various concentrations. The ratio of R_g (Radius of Gyration)/R_h (Hydrodynamic Radius Distribution) is used to describe the shape and extension degree of the molecular chain in the solution; it is widely used in the study of single chain and aggregations in polymer solution. Therein, R_g is the root-mean-square radius of gyration; it reflects the real size of molecular chain. If the value of z-average radius of gyration (R_g)/ average hydrodynamic radius (R_h) is big, the structure of polymer chain emerges with extended and loose; if the value R_g/R_h is small, the structure of polymer chain emerges with compact packing. According to the relevant reports,[15] the chain conformations show extend rod, random coil and hyper branched cluster respectively when R_g/R_h are in 2.0, 1.5~1.8, 1.0~1.2, so the structure of chain becomes more and more compact with concentration increases. From Table 2, it was found that the average R_g was enhanced from 21.0 nm to 31.3 nm with concentration decrease from 5.0 to 0.5 mg/mL, it indicated the chains size was gradually increased; simultaneously, the R_h was also enhanced from 10.5 nm to 7.0 nm. But the R_g/R_h behaved just oppositely, the value was slightly reduced from 4.47 to 2.00 with the increase of solution concentrations in the $CHCl_3$. Therefore, they were "extended and stacked rod" like structures in solvent $CHCl_3$. For the PPFOH in THF solutions, all R_g, R_h and R_g/R_h behaved show similar tendency to PPFOH/$CHCl_3$ solutions with increasing concentrations. However, the ratio of R_g/R_h is significantly reduced from 2.43 to 1.06 with the increase of solution concentrations from 0.5 mg/mL to 5 mg/mL, suggested the chain exhibited "random coil/hyper branched cluster or Globule" in the solution states.

Table 2. Conformational parameters of PPFOH in two type solutions.

Concentration	$CHCl_3$			THF		
mg/mL	R_g (nm)	R_h (nm)	R_g/R_h	R_g (nm)	R_h (nm)	R_g/R_h
0.1	48.7	/	/	18.3	/	/
0.5	31.3	7.0	4.47	18.2	7.5	2.43
1.0	24.0	7.4	3.24	15.9	7.5	2.12
5.0	21.0	10.5	2.00	15.0	14.2	1.06

Further investigation of the PPFOH aggregation behavior in the $CHCl_3$ (Type I solvent) and THF (Type II solvent) solutions and

films are also shown here (Figure 2a). A strong Tyndall effect was observed in the 5 mg/ml concentrated $CHCl_3$ solution using a 628 nm laser diode to excite the sample, indicated that the largest effective dynamic radius of PPFOH "aggregate" is similar or smaller than the laser wavelength value (Figures 2a and S8). However, when the laser light excited the sample of PPFOH THF solution, there was different from ones in the $CHCl_3$ solution, this could be that aggregate in the THF solution has a larger hydrodynamic radius than the wavelength value of laser source. Meanwhile, from DLS results, compared with PPFOH aggregate in the $CHCl_3$ solution, the correlation function of PPFOH in THF solution is shifted to a longer time scale shown in Figure 2a. The R_h spectra distribution of $CHCl_3$ solution appears up to three relaxation modes. The fast and mostly mode with the average R_h of PPFOH in $CHCl_3$ solution about ~30 nm, representing the translational diffusion of individual PPFOH chains, while the intermediate and the slow mode with the larger R_h distributions of about ~30 nm and 300 nm (less than wavelength of laser source, 628 nm) are attributed to the internal motions of hydrogen-bond-assisted aggregates.[21] The R_h spectra distribution of PPFOH in the THF solution (5 mg/ml) also consisted of three peaks with the lower R_h of about ~20 nm and ~300 nm, attributing to the individual PPFOH chains and nanoscale-aggregate, together with an additional relaxation and slowest mode with the larger R_h ranging to *ca.*~1.5 μm.[16] Therefere, it is concluded that PPFOH has larger-scale random aggregation in type II solutions than in type I solutions. In this regard, polymer chains showed folded and tangled conformational orders in “Globule” or hyper branched cluster type aggregate solution for the stronger non-covalent interaction between polymer chain and THF molecules. Besides, the aggregations from the interchain interaction in the solution states that polymer chains exhibited extended and stacked rod type aggregates in the solution, and further form a packed and cross-linked polymer superstructure in the film.

Nanoscale infrared technique, called in-situ atomic force microscope infrared tool (AFM-IR), was explored here to further investigate the PPFOH film morphologies spun from type I and type II solutions (Figures 2e-2f and S9). From the AFM images (Figure 2c), a spun film from the $CHCl_3$ solution shows small grains with an average roughness of 0.68 nm. Meanwhile, there are small domains with the size of ~200 nm in the film, similar to the slow mode "R_h" value of network aggregates in the precursor solution (Figure 2a). For the films spin-coated from THF solution, the surface roughness is increased to 1.39 nm. And much larger scale "heterogeneities" with several hundred nanometers in size, were observed (Figure 2b), similar to the nanoscale-phase separation in the bulk heterojunction films for a multi-components system. Thus, the aggregate in a precursor solution may maintain in such solution processed films as the “guest” and induce self-dopant formation. Furthermore, FTIR spectra were measured on PPFOH power to compare with AFM-IR spectra on the thin films to assess the function of hydroxyl groups. It is well known that the -OH stretching bands can be used to screen the formation of hydrogen bonds. The FTIR spectra of PPFOH powders are shown in Figure S9 that there are two peaks at 3550 and 3450 cm^{-1}, which are featured for the hydroxyl group, suggesting the existence of free and associated hydroxyl groups. Moreover, AFM-IR spectra of PPFOH films coated from $CHCl_3$ at two recorded locate sites (both A and B sites), have two similar peaks to the FTIR spectra at the wavenumbers of about 3500 and 3400 cm^{-1}, respectively, indicating free or associated with OH groups. The film morphology is relatively homogeneous. However, only lower wavenumber peak at 3392 cm^{-1} is observed in the AFM-IR spectrum of the PPFOH spin-coated film from THF solution at site C. This can be explained for the dominant associated hydroxyl groups in the film states. It was also found that there is a mixed IR absorption band with a less distinctive peak at 3516 cm^{-1} associated with free -OH, and 3460 & 3400 (associated -OH) cm^{-1} at site D, revealing that the hydrogen-bond interaction is stronger at C site than those of D site. The lower percentage of freedom -OH group at C and D in the type I films than A and B in the type II films further confirms that there is stronger interchain hydrogen-bonding interaction in the type I films than those of type II films. Furthermore, their hydrophilic and hydrophobic properties (Figures 2c, 2d and S10) are analyzed here to explore the distribution of hydroxyl group. The water

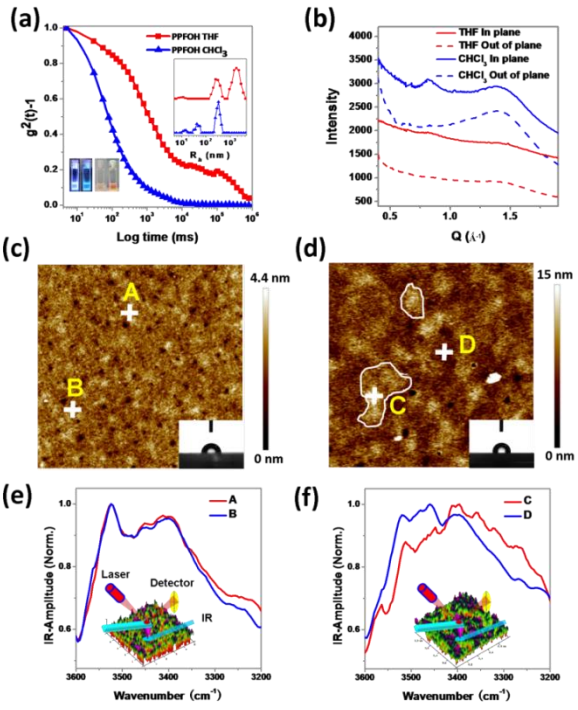

Figure 2. (a) Normalized intensity correlation function, $g^2(t)$-1, and the hydrodynamic radius (R_h) distribution (inset) of two type PPFOH solutions. Inset show the photographs of PPFOH THF and $CHCl_3$ solution (5 mg/ml) under UV lamp (365 nm) and their Tyndall effect (Laser wavelength is 628 nm.). (b) 1D GIXD profiles of PPFOH films spin-coated from THF and $CHCl_3$ solution. AFM images and Nanoscale infrared analysis technique (AFM-IR) spectra of PPFOH spin-coated films from $CHCl_3$ (c, e) and THF (d, f) solution. AFM images scale is 5 × 5

μm. Film thicknesses are both about 70~80 nm. Inset show the scheme of the AFM-IR measurements.

Table 3. Performance of PPFOH-based thin-film devices.

Polymer	Solvents	V_{on}/V^a	C. E.[b]	$L_{max}{}^c$	λ/nm[d]	CIE[e]	Color
PPFOH-L	Type I: $CHCl_3$ (A)	5.21	0.82 (6.5)	156	444, 536	0.24, 0.26	Blue
	Type II: THF (B)	5.30	0.53 (7.5)	394	456, 524	0.26, 0.29	Sky Blue
PPFOH	Type I: $CHCl_3$ (C)	5.50	0.82 (7.0)	465	440, 560	0.33, 0.35	White
	Type II: THF (D)	6.60	1.10 (9.2)	1303	536	0.37, 0.50	Green
PPFOH-H	Type I: $CHCl_3$ (E)	6.00	0.93 (7.5)	420	594	0.51, 0.46	Orange
	Type II: THF (F)	7.35	0.59 (10.0)	660	565	0.47, 0.46	Yellow

[a]Turn-on voltage at 1 cd/m^2. [b]Maximum current efficiency (C. E.). [c]Maximum luminance. [d]Wavelength of emission peak at 2 mA/cm^2. [e]CIE coordinate of EL spectra at 2 mA/cm^2.

contact angle on the PPFOH film spin-coated from $CHCl_3$ is ~95° with the surface energy of 26.12 mN/n. It is a typical value for hydrophobic polymer films. And PPFOH films spin-coated from THF solution have a greater hydrophobicity with a water contact angle of ~105° and surface energy of 23.7 mN/n. In other words, the increased hydrophilicity of PPFOH film spin-coated from $CHCl_3$ means more number of free hydroxyl groups (hydrophilic hydroxyl group) than PPFOH films spin-coated from THF solutions. It should mention that the increased hydrophobicity may also attribute to the larger film roughness. Therefore, there is weaker hydrogen-bonding interaction in the type I films than those in type II films, which leads to a stronger interchain aggregation.

Tunable Electroluminescence (EL) Colors of PPFOH via Supramolecular Approach. Non-covalent interactions allow for PPFOH polymer to have multi-color emissions in solution and solid states. In this section, we will fabricate multi-color PPFOH-based PLEDs via controlling the molecular aggregations. Firstly, PPFOH emissive layer (EML) was spin-coated from varied solutions with the fixed concentration of 5 mg/ml on the top of poly (3, 4-ethy-lenedioxythiophene): poly(styrene sulfonate) (PEDOT: PSS) as a hole injection layer. Indium tin oxide (ITO) was used as the anode electrode. The electron-transporting layer of 1,3,5-tris(N-phenylbenziphenyl benzimidazol-2-yl)benzene (TPBi) and LiF were thermally deposited on the top of the PPFOH layer. So the EL device structure has a configuration of ITO/PEDOT: PSS (40 nm)/PPFOH (60~70 nm) /TPBI (40 nm)/LiF (0.6 nm)/Al (80 nm).

It is well known that the intensity of hydrogen-bonding interaction is significantly depended on polymer molecular weight (M_n). In this work, we also prepared two extra PPFOH with the different M_n and PDI, labelling with PPFOH-L and PPFOH-H, which M_n and PDI are 1.04 × 10^4 & 2.12 and 3.48 ×10^4 & 1.33, respectively (Figure S1). Besides, our normal one labelled with PPFOH above. The degrees of polymerization (DP) are estimated to be *c. a.* 26 for PPFOH-L and *c. a.* 90 for PPFOH-H. Moreover, the emission peaks of PPFOH-H films are not only red-shifted but also has a stronger emission intensity at longer wavelength compared with the emissions of PPFOH and PPFOH-L (Figures 3a and 3b), indicating that a higher M_n has stronger hydrogen bonding interaction and energy transfer. Therefore, the emission colors of PPFOHs films can be tuned from blue, sky blue, and green, green-yellow, yellow to pink via controlling M_n and selective solvents (Figure 3b).

Device performances of PPFOHs-based PLEDs are shown in **Figurs 3**, S11 and **Table 3**. Similar to their film PL spectra, EL spectra consisted of two emitting regions: blue emission (440~460 nm) and yellow-green emission (540~600 nm). However, EL spectra of the PPFOH films made from THF solutions exhibit a sky-blue emission with the maximum peak of 456 nm with a shoulder low-band emission at 524 nm. High-energy emission (440~460 nm) from the PPFOH backbone chain (host) are quenched, showing a weaker peak at 440 nm along with a strong emission at 536 nm (green light). And emission for PPFOH-H films has red-shifted to 565 nm (yellow light) and its blue emission almost disappeared, indicating that self-doping energy transfer within the films is nearly completed. The CIE coordinates of the EL spectra for PPFOH-L, PPFOH and PPFOH-H films spin-coated from THF solutions are about (0.26, 0.29), (0.37, 0.50), (0.47, 0.46) at 2 mA m^{-2}, respectively. Interestingly, EL from the PPFOH-L thin film spin-coated from $CHCl_3$ solution shows a blue emission with the CIE of (0.24, 0.26) indicating weaker energy transfer than those of films spin-coated from THF solutions. However, the main emission peaks in the EL spectra of PPFOH films from $CHCl_3$ solutions are about 440 and 560 nm at 2 mA m^{-2} with the CIE coordinates of (0.33, 0.35) (white light). And the EL from PPFOH-H films made from $CHCl_3$ solution changes to orange color because its blue emission at 440 nm has significantly decreased, showing a strong emission at 594 nm with the CIE coordinates of (0.51, 0.46). Therefore, the color-tunable supramolecular EL spectra have been successfully tuned from blue, sky blue, nearly white, green orange and yellow via controlling energy transfer in self-doped films (Figure 3d).

EL devices made from PPFOH-L, PPFOH and PPFOH-H films spin-coated from $CHCl_3$ and THF solutions are labeled as device A and B, C and D, E and F, respectively, which the devices performance are summarized in Figure 3e, 3f and Table 2. It can be seen that the turn-on voltages (V_{on}) for the devices A and B are 5.21 and 5.30 V, respectively. These two devices have lower turn-on voltages than those of the other devices. Both device A and device B exhibit the maximum brightness of 156 cd m^{-2} and 394 cd m^{-2} with the maximum current efficiency (C. E) of 0.82 cd/A at 6.5 V and 0.53 cd/A at 7.5 V, respectively. The turn on voltage of the devices C and E are about 5.50 and 6.0 V with the maximum brightness of 465 and 420 cd m^{-2}, and their maximum current efficiencies are 0.82 and 0.93 cd/A at the voltages of 7.0 and 7.5 V, respectively. The devices D and F, have the turn-on voltages are about 6.6

and 7.35 V, maximum brightness of 1303 and 660 cd m^{-2}, maximum C. E of 1.10 cd/A and 0.59 cd/A at the voltages of 9.2 and 10.0 V, respectively. Now we can summarize that the color-tunable EL can be achieved using a single-component polymer via supramolecular approach.

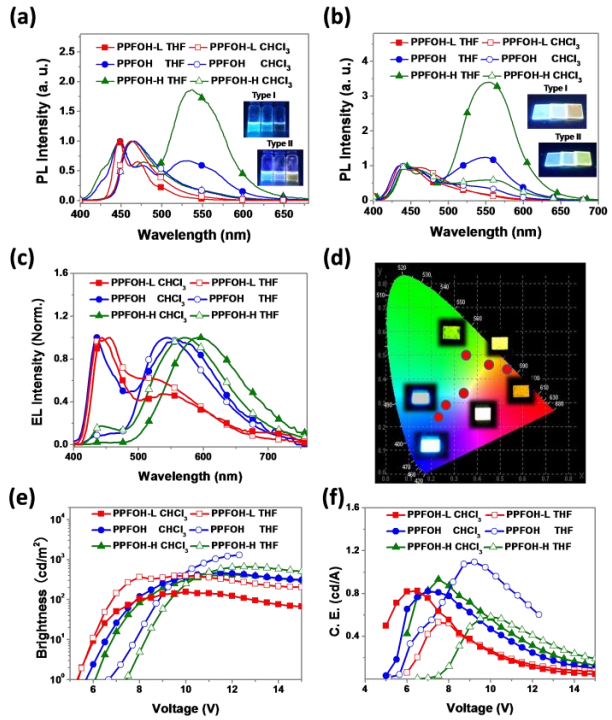

Figure 3. (a) PL spectra of PPFOHs various concentrated solutions (5 mg/ml) and corresponding spin-coated films (b). Supramolecular EL spectra (c) and CIE coordinate (d) of thin film devices, together with brightness density (e) and current efficiency (C. E.) (f) versus voltage curve.

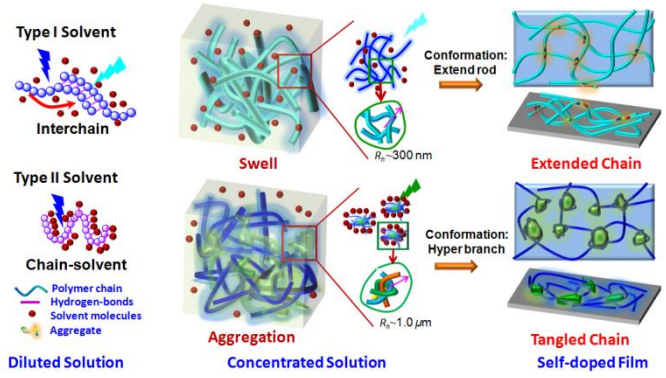

Scheme 1. Schematic illustration of two type PPFOH aggregation structure in the solution and film states.

Discussion. Actually, the fundamental role solvent plays in dictating polymer conformation and aggregation have been known and studied since the early work of Flory. Polymer chain can self-organize into multi-dimensional superstructure in solution states, which may effect by the solvent quality, solubility, solvent-chain interaction as well as side-chain/ side-chain interactions. Significantly different to common and simpler plastics or glass, CPs encompasses a broad spectrum of electrostatic and dispersion interactions, which are also influenced by the diverse non-covalent interactions among chain-chain, side chain-side chain or solvent molecules-chain etc. While backbone linearity is one fundamental determinant of ordered conformational class formation, the ability of these molecules to form π-stacks can be influenced by the dihedral angle distribution of the polymer, which incorporates both the monomer-monomer torsional potential, as well as side-chain/ side-chain interactions. In this regard, it is not surprising that PPFOH with the diverse hydroxyl units had complicated aggregation behavior and programmed optoelectrical property. PPFOH interchain complexes does exist in the type I diluted solution for the formation of interchain hydrogen-bonding interactions. In the type II solutions, it may form a chain-solvent molecular complex (called as amphiphilic PPFOH@solvent complexes in solution, similar to rod-coil systems) for a hydrogen-bonding interaction between polymer chain and solvent molecule rather than interchain ones (***Scheme 1***). With increasing the concentrations, the interchain complex can self-assemble into a cross-linked gelation aggregate that the polymer chains could align and stack at nanoscale in the type I solvent solution. However, as the result of PPFOH@solvent complex's amphiphilic property, polymer chains can self-assemble into a larger “globule or hyper branch”-type aggregate, which is consisted of hydroxyl groups on outmost and backbone structure in the core, and further result into a strong interchain interaction and aggregation.[14, 17] These diverse conformational orders in the aggregates of PPFOH may propagate into the mesoscale morphology of films states from the fast solvent evaporation.[3b, 6b] As shown in *Scheme* 1, the packed polymer complex from a precursor of the cross-linked network structure may maintain in the film-processing but also show a stronger hydrogen-bonding interaction due to the fast solvent evaporation than those in the solution states, resulting in a low-band emission at 520-560 nm. More strong aggregation and larger-scale complex from a slightly “amphiphilic” property of PPFOH chains in the type II solutions may explain the sharp and strong emission at 525~530 nm. The GIXD pattern (Figure 2b and S12) gives an evidence that the PPFOH interchain *π-π* interaction (d=4.498 Å) in the spin-coated films made from $CHCl_3$ solution is slightly stronger than those in films made from THF solution (no obvious *π-π* interaction pattern was observed), confirming the stronger chain (fluorene) packed or stacked in the type I aggregate (shown in *Scheme 1*). However, PPFOH chains in the type II films show stronger interchain hydrogen bonding interaction but a weaker *π-π* interaction than those in the type I films. Consequently, we will divide into two parts to further discuss the origin of two type aggregation behavior and low-band emission: **(1) PPFOH Materials without Oxidation.** We proposed that, PPFOH chains as shown into *Scheme* 1 exhibit significantly folded, bended and distorted conformational orders in the THF solution states and corresponding films, indicating that the distorted and folded fluorene conformation may be the original low-band emission similar to the previous reports.[18] Highly strained [4]cyclofluorene can show a strong emission at low-band energy with the range from 500~600 nm, further confirmed that the distorted fluorene conformation may induce a green-band emission in polyfluorene under an

extreme aggregation.[19] To some extent, the origin of the type II films emitting with a narrow low-band emission at 520~540 nm may attribute to the molecular distortion of fluorene monomer induced by a strong inter- and intramolecular hydrogen-bonding interaction. Moreover, the dimer of fluorene can also have the type II low-band emission at 540~560 nm. **(2) PPFOH Materials with Oxidation.** Actually, all aromatic polymers cannot completely avoid the oxidation in the preparation and purification processing, especial under the O_2, H_2O and daylight. In this work, our PPFOH also cannot completely avoid the oxidation. In this regard, green band emission at 530 nm for type II film and 560 nm for type I may be also attributed to single PPFOH-*co*-fluorenone isotropic states and fluorenone excimer, respectively. Even more, our experimental results also indicated that there is different aggregation behavior of so-called PPFOH-*co*-fluorenone in solution states. Interchain hydrogen-bonding interaction, rather than interaction between chain and solvent, tends to induce excimer formation.

Conclusions

In summary, we systematically investigated the role of supramolecular interaction in the self-organization behavior and photophysical properties of supramolecular polyfluorenols. Firstly, chain aggregations driven from the secondary interaction between chain and solvent molecules in the precursor solutions that leads to the polymer chains having slightly "amphiphilic" property (rod-coil) which may form “Globule or hyper branch” type aggregates, and further allow the chains for strong folded, tied and tangled conformational orders in the post-processed film states. Secondly, polymer chains can self-assemble into “Stacked rod” type aggregates in the solution for the interchain interaction, and further form a packed and cross-linked polymer superstructure in the films. Finally, EL colors of our supramolecular conjugated polymer can be tune from blue, sky blue, near white, green, and yellow to orange. Consideration of the synergistic effects of non-covalent interaction in a precursor solution and exquisite control of aggregation can precisely optimize chain arrangement in solid states, thereby constructing a high quality film for printed electronic devices.

Acknowledgements

The work was supported by the National Key Basic Research Program of China (973) (2015CB932200), National Natural Science Foundation of China (21504041, 21502091, U1301243), Six Peak Talents Foundation of Jiangsu Province (XCL-CXTD-009), Dr Jinyi Lin thanks SICAM Fellowship, Oxford University and Imperial College London. Dr Xuhua Wang gratefully acknowledges the Plastic Electronics Centre for Doctoral Training, UK EPSRC (EP/G037515/1). Professor Donal Bradley also thanks the University of Oxford.

Notes and references

1 a) J. H. Burroughes, D. D. C. Bradley, A. R. Brown, R. N. Marks, K. Mackay, R. H. Friend, P. L. Burns, A. B. Holmes, *Nature*, 1990, **347**, 539-541. b) M. Campoy-Quiles, T. Ferenczi, T. Agostinelli, P. G. Etchegoin, Y. Kim, T. D. Anthopoulos, P. N. Stavrinou, D. D. C. Bradley, J. Nelson, *Nature Mater.*, 2008, **7**, 158-164. c) M. Grell, D. D. C. Bradley, *Adv. Mater.*, 1999, **11**, 895-905. d) L.-H. Xie, C.-R. Yin, W.-Y. Lai, Q.-L. Fan, W. Huang, *Prog. Polym. Sci.*, 2012, **37**, 1192-1264.

2 a) F. Liu, Y. Gu, X. Shen, S. Ferdous, H.-W. Wang, T. P. Russell, *Prog. Polym. Sci.*, 2013, **38**, 1990-2052. b) J. D. A. Lin, O. V. Mikhnenko, T. S. van der Poll, G. C. Bazan, T.-Q. Nguyen, *Adv. Mater.*, 2015, **27**, 2528-2532.

3 a) R. Noriega, J. Rivnay, K. Vandewal, F. P. V. Koch, N. Stingelin, P. Smith, M. F. Toney, A. Salleo, *Nature Mater.*, 2013, **12**, 1038-1044. b) B.-G. Kim, E. J. Jeong, J. W. Chung, S. Seo, B. Koo, J. Kim, *Nature Mater.*, 2013, **12**, 659-664. c) M. Knaapila, A. P. Monkman, *Adv. Mater.*, 2013, **25**, 1090-1108.

4 a) M. Grell, D. D. C. Bradley, X. Long, T. Chamberlain, M. Inbasekaran, E. P. Woo, M. Soliman, *Acta Polym.*, 1998, **49**, 439-444. b) J.-Y. Lin, W.-S. Zhu, F. Liu, L.-H. Xie, L. Zhang, R. Xia, G.-C. Xing, W. Huang, *Macromolecules*, 2014, **47**, 1001-1007. c) T. Fu, Z. Li, Z. Zhang, X. Zhang and F. Wang, *Macromolecules*, 2017, **50**, 7517-7525.

5 a) A. Perevedentsev, N. Chander, J.-S. Kim, D. D. C. Bradley, *J. Polym. Sci. Part B: Polym. Phys.*, 2016, **54**, 1995-2006. b) H. Ling, J. Lin, M. Yi, B. Liu, W. Li, Z. Lin, L. Xie, Y. Bao, F. Guo, W. Huang, *ACS Appl. Mater. & Interfaces*, 2016, **8**, 18969-18977. c) B. Liu, J. Lin, F. Liu, M. Yu, X. Zhang, R. Xia, T. Yang, Y. Fang, L. Xie, W. Huang, *ACS Appl. Mater. & Interfaces*, 2016, **8**, 21648-21655. d) H.-H. Lu, C.-Y. Liu, C.-H. Chang, S.-A. Chen, *Adv. Mater.*, 2007, **19**, 2574-2579.

6 a) J. Lin, Z. Yu, W. Zhu, G. Xing, Z. Lin, S. Yang, L. Xie, C. Niu, W. Huang, *Polym. Chem.*, 2013, **4**, 477-483. b) K. Schmidt, C. J. Tassone, J. R. Niskala, A. T. Yiu, O. P. Lee, T. M. Weiss, C. Wang, J. M. J. Frechet, P. M. Beaujuge, M. F. Toney, *Adv. Mater.*, 2014, **26**, 300-305. c) W. Ma, G. Yang, K. Jiang, J. H. Carpenter, Y. Wu, X. Meng, T. McAfee, J. Zhao, C. Zhu, C. Wang, H. Ade, H. Yan, *Adv. Energy Mater.*, 2015, **5**. 15014000. d) Y. Liu, J. Zhao, Z. Li, C. Mu, W. Ma, H. Hu, K. Jiang, H. Lin, H. Ade, H. Yan, *Nature Commun.*, **2014**, **5**, 5293. e) J.-Y. Lin, B. Liu, M.-N. Yu, C.-J. Ou, Z.-F. Lei, F. Liu, X.-H. Wang, L.-H. Xie, W.-S. Zhu, H.-F. Ling, X.-W. Zhang, P. N. Stavrinou, J.-P. Wang, D. D. C. Bradley, W. Huang, *J. Mater. Chem. C*, 2017, **5**, 6762-6770. f) J.-H. Chen, C.-S. Chang, Y.-X. Chang, C.-Y. Chen, H.-L. Chen, S.-A. Chen, *Macromolecules*, 2009, **42**, 1306-1314. g) M.-N. Yu, B. Liu, J.-y. Lin, T. Li, D. Lu, F. Liu, W.-s. Zhu, L.-h. Xie, W. Huang, *Chinese J. Polym. Sci.*, 2016, **34**, 1311-1318. h) J.-Y. Lin, G.-Y. Zhu, B. Liu, M.-N. Yu, X.-H. Wang, L. Wang, W.-S. Zhu, L.-H. Xie, C.-X. Xu, J.-P. Wang, P. N. Stavrinou, D. D. C. Bradley and W. Huang, *ACS Macro Lett.*, 2016, **5**, 967-971.

7 a) J. Kim, T. M. Swager, *Nature*, 2001, **411**, 1030-1034. b) E. Collini, G. D. Scholes, *Science*, 2009, **323**, 369-373.

8 a) F. J. M. Hoeben, P. Jonkheijm, E. W. Meijer, A. Schenning, *Chem. Rev.*, 2005, **105**, 1491-1546. 26. b) D. M. Bassani, L. Jonusauskaite, A. Lavie-Cambot, N. D. McClenaghan, J.-L. Pozzo, D. Ray, G. Vives, *Coord. Chem. Rev.*, 2010, **254**, 2429-2445. c) A. J. Heeger, *Chem. Soc. Rev.*, 2010, **39**, 2354-2371. d) R. C. Evans, *J. Mater. Chem. C*, 2013, **1**, 4190-4200. e) Y.-K. Tian, Y.-F. Han, Z.-S. Yang and F. Wang, *Macromolecules*, 2016, **49**, 6455-6461.

9 a) T. Aida, E. W. Meijer, S. I. Stupp, *Science*, 2012, **335**, 813-817. b) J.-Y. Lin, J. Wong, L.-H. Xie, X.-C. Dong, H. Y. Yang, W. Huang, *Macromol. Rapid Commun.*, 2014, **35**, 895-900.

c) N. E. Jackson, B. M. Savoie, K. L. Kohlstedt, M. O. de la Cruz, G. C. Schatz, L. X. Chen, M. A. Ratner, *J. Am. Chem. Soc.*, 2013, **135**, 10475-10483.

10 a) J. Cornil, A. J. Heeger, J. L. Bredas, *Chem. Phys. Lett.*, 1997, **272**, 463-470. b) J. Cornil, D. A. dos Santos, X. Crispin, R. Silbey, J. L. Bredas, *J. Am. Chem. Soc.*, 1998, **120**, 1289-1299. c) F. Cacialli, J. S. Wilson, J. J. Michels, C. Daniel, C. Silva, R. H. Friend, N. Severin, P. Samori, J. P. Rabe, M. J. O'Connell, P. N. Taylor, H. L. Anderson, *Nature Mater.*, 2002, **1**, 160-164. d) F. C. Spano and C. Silva, in *Annual Rev. Phys. Chem., Vol 65*, eds. M. A. Johnson, T. J. Martinez, 2014, vol. **65**, 477-500.

11 a) J. J. van Franeker, M. Turbiez, W. Li, M. M. Wienk, R. A. J. Janssen, *Nature Commun.*, 2015, **6**, 6229. b) M. Yu, B. Liu, J. Lin, L. Bai, H. Ling, W. Zhu, L. Xie, M. Yi, J. Wang, W. Huang, *Rsc Adv.*, 2017, **7**, 14688-14693. c) Z.-Q. Lin, N.-E. Shi, Y.-B. Li, D. Qiu, L. Zhang, J.-Y. Lin, J.-F. Zhao, C. Wang, L.-H. Xie, W. Huang, *J. Phys. Chem. C*, 2011, **115**, 4418-4424.

12 Hayer, A. L. T. Khan, R. H. Friend, A. Kohler, *Phys. Rev. B*, 2005, **71**, 241302.

13 W. Zhao, T. Cao, J. M. White, *Adv. Funct. Mater.*, 2004, **14**, 783-790.

14 a) Y. Koizumi, S. Seki, S. Tsukuda, S. Sakamoto, S. Tagawa, *J. Am. Chem. Soc.*, 2006, **128**, 9036-9037. b) L. Zhu, J. Qin, C. Yang, *J. Phys. Chem. B*, 2010, **114**, 14884-14889.

15 A. Z. Niu, D. J. Liaw, H. C. Sang, C. Wu, *Macromolecules*, 2000, **33**, 3492-3494.

16 L. Huang, L. Zhang, X. Huang, T. Li, B. Liu, D. Lu, *J. Phys. Chem. B*, 2014, **118**, 791-799.

17 N. E. Jackson, K. L. Kohlstedt, B. M. Savoie, M. O. de la Cruz, G. C. Schatz, L. X. Chen, M. A. Ratner, *J. Am. Chem. Soc.*, 2015, **137**, 6254-6262.

18 a) T. Adachi, J. Vogelsang, J. M. Lupton, *J. Phys. Chem. Lett.*, 2014, **5**, 2165-2170. b) D. Y. Yoo, T. Nguyen Dien Kha, S. L. Lee, E. Lee, S.-R. Jeon, S. Hwang, H. S. Lim, J. K. Kim, B. K. Ju, H. Kim, J. A. Lim, *ACS Nano*, 2014, **8**, 4248-4256.

19 Y.-Y. Liu, J.-Y. Lin, Y.-F. Bo, L.-H. Xie, M.-D. Yi, X.-W. Zhang, H.-M. Zhang, T.-P. Loh, W. Huang, *Org. Lett.*, 2016, **18**, 172-175.